Advances in Computational Design, *Vol. 11, No. 2 (2026) 171-187*
https://doi.org/10.12989/acd.2026.11.2.171

Bio-inspired helicoidal layered structures for enhanced energy absorption: A finite element comparative study

Navaneeth V.[1], Aswanipriya K. V.[1], Golak Bihari Mahanta[2], Piyush Pratap Singh*[1]

[1]*Department of Mechanical Engineering, Amrita School of Engineering, Amrita Vishwa Vidyapeetham, Chennai, India*
[2]*Mechatronics and Automation Engineering, National Institute of Technology, Patna, India*

(Received December 19, 2025, Revised March 2, 2026, Accepted April 7, 2026)

Abstract. Bio-Inspired Structures have become a significant research direction for developing sustainable Structural components with lightweight yet damage tolerant, and energy efficient designs. Among these Structures, one of the most prominent ones is the Bouligand-type Helicoidal structures which are characterized by their linear and gradual rotation of layers between each layer. They've shown a high resistance to fracture and improvised energy dissipation capabilities. while significant number of studies were conducted to examine their high strain-rate impact behavior, their response to gradual loading are has not been full studied. To address this gap, the present work involves in performing an investigation of Bouligand-type structures under quasi static loading using Ansys. In this study, four such Bio-inspired structures were studied out of those four, three of them are helicoidal structures (Bouligand-type) with different angle of layer rotations and the other one is Honeycomb Structure. All these structures are assigned epoxy-carbon (395 GPa) composite material to ensure consistent mechanical assumptions across all the cases. All of those structures are designed and sandwiched between two plates. A Controlled displacement ranging from 0-10 mm was applied to the top surface which is generally the plate in a quasi-static Approach, while the bottom plate is fixed. In addition to compression, a displacement-controlled flexural analysis was conducted to evaluate the structural performance under bending action and to represent more realistic service loading conditions. Frictional effects were neglected to maintain computational stability and to solely focus on the structural response.

Keywords: bio-inspired structures; finite element analysis; geometric modelling and analysis; modelling and simulation; quasi-static analysis; simulation based design

1. Introduction

The development of lightweight structural systems which are capable of sustaining progressive deformation while maintaining high energy absorption has been a key objective in field of aerospace, automotive, and protective engineering applications. Conventional laminated composites, although widely preferred due to their high specific stiffness and strength, it often exhibits a brittle failure mechanism such as sudden crack propagation and interlaminar delamination under quasi-static loading conditions. Numerical investigations have demonstrated that these structural architecture plays a dominant role in governing stiffness, stress redistribution, and strain energy

*Corresponding author, Assistant Professor, E-mail: piyushpratap12@gmail.com

http://www.techno-press.org/acd/5
ISSN: 2383-8477 (Print), 2466-0523 (Online)

accumulation. In particular, Nguyen et al. [1] showed through a continuum-based numerical modelling that modifying its internal structural configuration alone can significantly alter the response of these composite structures without changing material properties.

Nature provides several examples of such architected structures that can overcome the limitations of conventional laminates through hierarchical design. Raabe et al. [2] demonstrated that the Crustacean exoskeleton (a biocomposite) that achieves exceptional toughness through a graded Bouligand-type fibrous arrangement that also promotes crack deflection and delayed failure. Inspired by such biological systems, helicoidal or Bouligand-type architectures have been incorporated into engineered composite laminates. Lee et al. [3] numerically showed that such layered and sandwich composite structures exhibit strong sensitivity to geometric arrangement under compressive loading condtions. These findings align with the biological observations reported by Weaver et al. [4], who revealed that the stomatopod dactyl club (a damage resistance biological structures found in crabs) has a highly ordered helicoidal architecture which capable of withstanding repeated extreme impacts without any major failures.

The mechanical advantages of such helicoidal architectures have been further investigated through fracture and damage studies. Suksangpanya et al. [5] demonstrated that twisting cracks in Bouligand structures significantly increases the fracture resistance by extending the crack path and reducing localized stress intensity. Incorporating this concept to engineered materials, Kim et al. [6] investigated architected composite structures under quasi-static compression and reported that rotational stacking sequences enable more uniform strain distribution and delayed deformation. Han et al. [7] further showed that these bio-inspired helicoidal laminates exhibits a superior impact resistance compared to conventional laminates due to their enhanced shear transfer between adjacent layers. A comprehensive review by Ning et al. [8] consolidated that these findings and highlighted that helicoidal composites improve interlaminar toughness and damage tolerance across a wide range of loading conditions.

In parallel with these layered architectures, cellular systems such as honeycomb cores are also widely used for energy absorption due to their predictable deformation patterns and high stiffness-to-weight efficiency. Al-Maliki et al. [9] numerically demonstrated the bending behaviour of composite structures under loading. These structures can undergo bending-dominated deformation with stress concentration at junctions under compressive loading. Wang et al. [10] further showed that these architected cellular materials when subjected to displacement-controlled loading can exhibit enhanced strain energy storage and its geometry promotes a progressive deformation. Although honeycomb structures offer a more stable load–displacement behavior, their localized deformation mechanisms differ from the distributed shear and twisting mechanisms that are observed in helicoidal laminates.

From mechanical performance and finite element study perspective, accurate prediction of these behaviors requires refined numerical formulations and complex finite element strategies. Narwariya et al. [11] Studied mesh sensitivity and numerical stabilization, which are critical when modelling thin-walled and architected structures to ensure reliable stress prediction. Adda Bedia et al. [12] demonstrated that finite element analysis of composite plates is highly sensitive to element formulation, mesh density, and interfacial assumptions under quasi-static loading. Bourada et al. [13] further showed that architectural configuration strongly governs stiffness and stress localization in laminated composites analyzed using refined theories, while Bousahla et al. [14] highlighted that stress and strain distribution in advanced composite systems are predominantly controlled by structural geometry rather than material anisotropy alone.

A finite element comparison between helicoidal layered cores with varying rotation angles and

conventional honeycomb cores under identical quasi-static compression conditions remains not being done. Most of these studies investigate architectures independently or under different modelling assumptions, making direct comparison difficult. Addressing this gap, the present study performs a finite element-based comparative analysis of three Bouligand-type helicoidal architectures with different rotation angles (30°, 45°, and 90°) and a honeycomb Structure using a uniformity-based modelling framework. By employing displacement-controlled loading, bonded interfacial conditions, and a verified mesh sensitivity study, this work aims to isolate architecture-driven deformation mechanisms and quantify their influence on deformation, stress localization, strain evolution, and strain energy absorption, consistent with established computational analyses of advanced composite structures as reported by Tounsi et al. [15].

2. Mathematical modeling

In this study, the quasi-static compressive response of the helicoidal and honeycomb cores is evaluated using a finite element formulation based on small-strain, linear elasticity. For a body occupying volume V with boundary surface S, Eq. (1) is the governing equation of equilibrium in the absence of inertial effects is expressed in the local (strong) form as

$$\nabla \cdot \sigma + b = 0 \tag{1}$$

where σ is the Cauchy stress tensor and b denotes the body force density.

Assuming small strains, the infinitesimal strain tensor

$$\varepsilon = \frac{1}{2}(\nabla u + (\nabla u)^T) \tag{2}$$

where u is the displacement field in Eq. (2). For a linear elastic material, the constitutive relation is written as

$$\sigma = C : \varepsilon \tag{3}$$

with C denoting the fourth-order elasticity tensor in Eq. (3) [12, 15]

Based on the principle of virtual work, the weak form of the equilibrium condition [15] for the quasi- static problem can be written as

$$\int_V \delta\varepsilon^T \sigma \, dV = \int_S \delta u^T t \, dS + \sum_{i=1}^{n} \delta u_i^T p_i \tag{4}$$

where δu and $\delta\varepsilon$ denote the virtual displacements and virtual strains, t represents the applied surface traction, and p_i are the concentrated nodal forces applied at n nodes.

Applying the finite element discretization and interpolating the displacement field within each element using suitable shape functions, Eq. (4) reduces to the standard linear algebraic system

$$[K]\{d\} = \{F\} \tag{5}$$

In Eq. (5) [K] is the global stiffness matrix assembled from the elemental contributions, {d} is the global displacement vector, and {F} denotes the equivalent nodal force vector.

In the present work, the bottom surface of each core is fully constrained, while a displacement-controlled compression is applied on the top surface. Since geometric nonlinearity is neglected, the

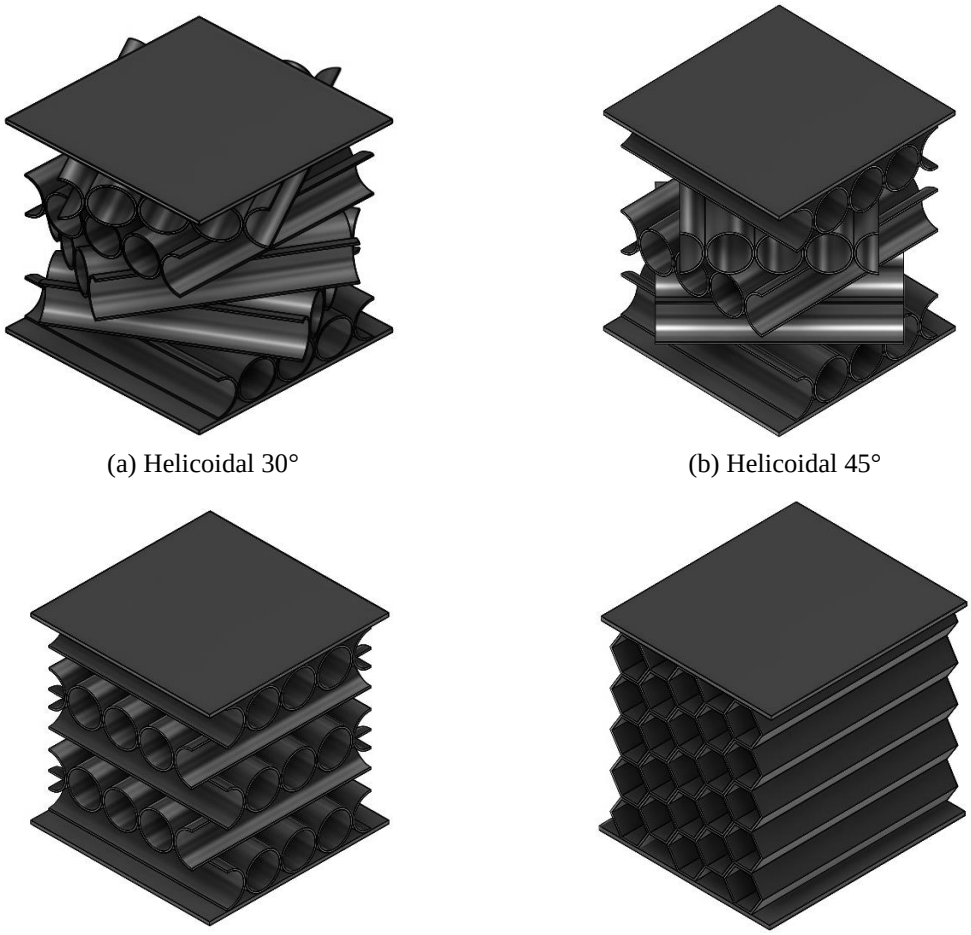

(a) Helicoidal 30° (b) Helicoidal 45°

(c) Helicoidal 90° d) Honeycomb Core

Figure 1. Geometric configurations of the four core architectures

governing equations remain linear, and the structural response is governed entirely by the material properties, geometry, and load paths of the helicoidal and honeycomb designs. The resulting stress, strain, and strain-energy fields obtained from the finite element solution provide quantitative insight into the deformation mechanisms and energy-absorption behavior of the different bio-inspired architectures.

3. Design of specimen cores

Naturally occurring biological systems exhibit highly optimal architecture that combines low density with exceptional mechanical robustness as shown in Fig. 1. Bouligand structures through their controlled fiber rotation across successive layers forces cracks to twist thereby increasing their dissipation and delay breaking Likewise, cuttlebone exhibits a periodic cellular frame of thin septa

Table 1. Geometric parameters

Parameter	Value
Plate length × width	10.00 × 10.00 mm
Core height	10 mm
Number of layers	5
Wall thickness	0.1 mm
Tube outer diameter	2.00 mm
Tube inner diameter	1.80 mm

and corrugated walls which are highly capable of withstanding extreme hydrostatic pressure its. despite low density. These design principles form the foundation for analyzing such bio-inspired structures, which can be used in many advanced engineering applications.

3.1 Helicoidal structural formulation

Inspired by the twisted-lamellar Bouligand arrangement show in Fig. 1(a)-(d) each helicoidal core is constructed from $N = 5$ stacked layers, where each layer is rotated by a constant increment $\Delta\theta$. The cumulative rotation of the *n*-th layer is given by Eq. (6)

$$\theta_n = \theta_0 + (n-1)\Delta \tag{6}$$

The structure height is maintained across all designs by dividing the core thickness H = 1

Each ply is a thin cylindrical shell with outer and inner diameters Do and Di; Eq. (7) gives the material cross- section per tube is

$$Atube = \pi \frac{D_o^2 - D_i^2}{4} \tag{7}$$

3.2 Honeycomb structural formulation

The honeycomb architecture shown in Fig. 1(d) represents a thin-walled cellular geometry, analogous to natural cellu- lar solids. Each regular hexagonal cell has side length a and wall thickness thc. For thin-walled hexagons, the solid wall area per cell is approximated by

$$A_{\text{hex, wall}} \approx 6\, a\, t_{hc} \tag{8}$$

When extruded through height *H*, the volume of solid material per cell becomes

$$V_{\text{hex,solid}} \approx 6\, a\, t_{hc}\, H \tag{9}$$

The relative density of the honeycomb structure used for architecture-normalized comparisons is

$$\rho_{rel} = \frac{V_{solid,core}}{L_x L_y H} \tag{10}$$

Eqs. (8-10) are derived based on classical thin-walled honeycomb formulations.

3.3 Design rationale

Table 1 shows the overall external dimensions (10 × 10 × 10 mm) Across all core types, number of layers, and wall thicknesses were kept constant to ensure a density-consistent comparison. The helicoidal designs emulate biological crack-twisting mechanisms, whereas the honeycomb design reflects efficient load distribution through thin cellular walls. The combined use of rotational lamellae and thin-walled cells mirrors design strategies observed in natural composites enabling a systematic investigation of how structural architecture alone governs quasi-static deformation and energy absorption.

4. Finite element modelling

4.1 Mesh generation

Meshes of both structures were created by using SOLID 185 tetrahedral elements, which is more suitable for modelling thin-walled geometries under linear elastic behaviour. Since the helicoidal tubes have very thin walls (0.1mm) and circular interfaces, achieving mesh uniformity and quantity was very critical. To obtain a stable and accurate solution, a system mesh study was incorporate by refining the mesh size iteratively and monitoring response parameters: overall stiffness K, peak equivalent stress σ_{eq}, and total strain energy U [11, 12]

Convergence was achieved with a nominal element size of $h = 0.35$ mm

This mesh density provided the sufficient resolution of tube curvature, wall thickness while maintaining reasonable fluctuations in the response parameters mentioned. During mesh verification, three quantities were used as indication for convergence:

Global stiffness

$$K_{eff} = \frac{F}{\delta} \tag{11}$$

where F is the reaction force and δ is the imposed displacement in Eq. (11).

4.2 Governing equations and output definitions

To evaluate the mechanical response of each structure during quasi-static compression, several standard continuum mechanics quantities were extracted from the FE solution.

Local stress analysis was performed using the von Mises equivalent stress:

$$\sigma_{eq} = \sqrt{\frac{1}{2}[(\sigma_1 - \sigma_2)^2 + (\sigma_2 - \sigma_3)^2 + (\sigma_3 - \sigma_1)^2]} \tag{12}$$

The corresponding equivalent strain is

$$\varepsilon_{eq} = \sqrt{\frac{2}{3}(E' : E')} \tag{13}$$

The transformed stiffness of a ply rotated by an angle θ is obtained from the relation:

$$Q = T^{-1}(\theta)\, Q_0\, T^{-T}(\theta) \tag{14}$$

Table 2. Material properties

Property	Symbol	Value
Young's Modulus	E	395 GPa
Poisson's Ratio	v	0.30
Density	ρ	1600 kg/m^3
Shear Modulus	G	152 GPa
Bulk Modulus	K	329 GPa

where Q is the reduced stiffness matrix, and T (θ) is the standard transformation matrix. These governing equations are more consistent with comparison of stiffness, deformation modes, and energy absorption across all these structures. Eq. (12-14) follow standard formulations from continuum mechanics and classical laminate theory.

4.3 Boundary and loading conditions

All these structures were designed as sandwiched between two plates.

• The bottom plate is fully fixed to prevent any rotational degree of freedom.

• The top plate was subject to a downward displacement of 10 mm, which is applied corresponding to each step, this process is carried out in 20 steps with incrementing the displacement 0.5 mm per step.

• This displacement-controlled loading replicates behavior that of a quasi-static compression test and ensures stable behavior.

• Any geometric non linearity was excluded (Large Deflection = OFF) since the primary focus is on the structural performance rather than simulating collapse mechanisms [13, 15].

4.4 Contact definitions

All interfaces were defined as bonded:

• Plate-core interfaces,

• Tube-tube interfaces,

• Layer-layer interfaces.

Bonded contact was applied between all the parts to ensure perfect load transfer and to prevent any relative motion between the layers, thereby maintaining linearity and numerical stability.

4.5 Material model

The Structures were assigned an epoxy–carbon composite material. The choice of material mainly due to its characteristics of reflecting realistic composite applications and it also provides high stiffness at relatively low density as shown in the Table 2. All simulations were performed using the same material to isolate effects of the material properties while comparing [14].

4.6 Extraction of mechanical response

• Total deformation

Table 3. Mesh sensitivity and result stabilization study for quasi-static compression

Case	Number of elements	Number of nodes	Maximum reaction force (N)	Deviation (%)
Mesh 1	6,200	42,500	3,385	–
Mesh 2	10,800	72,300	3,455	2.07
Mesh 3	15,400	108,900	3,508	1.53
Mesh 4	19,548	135,587	3,526	0.51
Mesh 5	22,562	161,930	3,529	0.09
Mesh 6	29,464	203,436	3,531	0.06

- Equivalent stress
- Equivalent strain
- Total strain energy

These outputs allow for the comparison of mechanical performance between those structural configurations. Contour distributions of σ_{eq}, ε_{eq}, and U were examined to visualize the stress pathways and energy absorption trends.

4.7 Mesh sensitivity and result stabilization study

A mesh sensitivity study was conducted to examine the influence of mesh density on the numerical response. As shown in Table 3, noticeable variations in the predicted reaction force are observed for coarse meshes. With progressive mesh refinement, the numerical response gradually stabilizes, and the deviation between successive meshes becomes negligible. In particular, the difference between the last three mesh configurations is less than 0.1%, indicating that the solution is essentially mesh- independent. Therefore, a mesh consisting of approximately 19,500 elements and 135,000 nodes was adopted for all subsequent analyses.

5. Results

5.1 Compressive response

5.1.1 Total deformation

Fig. 2(a-d) Demonstrates Deformation response of those four structural configurations was evaluated under a quasi-static compressive displacement of 10 mm. the obtained results as follows for 10.516 mm for 30° heli- coidal configuration, 10.397 mm for 45° helicoidal configuration, 10.023 mm for 90° configuration, and 10.405 mm for Honeycomb structure. Although the absolute difference on a numerical note is small, the trend is mechanically consistent with the deformational behaviour reported in bio-inspired layered architectures. The 30° structural configuration exhibited the highest deformation, confirm- ing its enhanced capacity for through-thickness distortion. This behaviour aligns with the currently existing studies proving that the smaller the rotational angle the higher will be the deformation. The 45° configuration had slightly reduced deformation but it also maintained similar response but with superior resistance due to its increase in angular stiffness. The honeycomb core, which traditionally praised for its high stiffness-to-weight ratio efficiency, demonstrated a deformation level that is close to the helicoidal 45°, mainly due to the characteristic

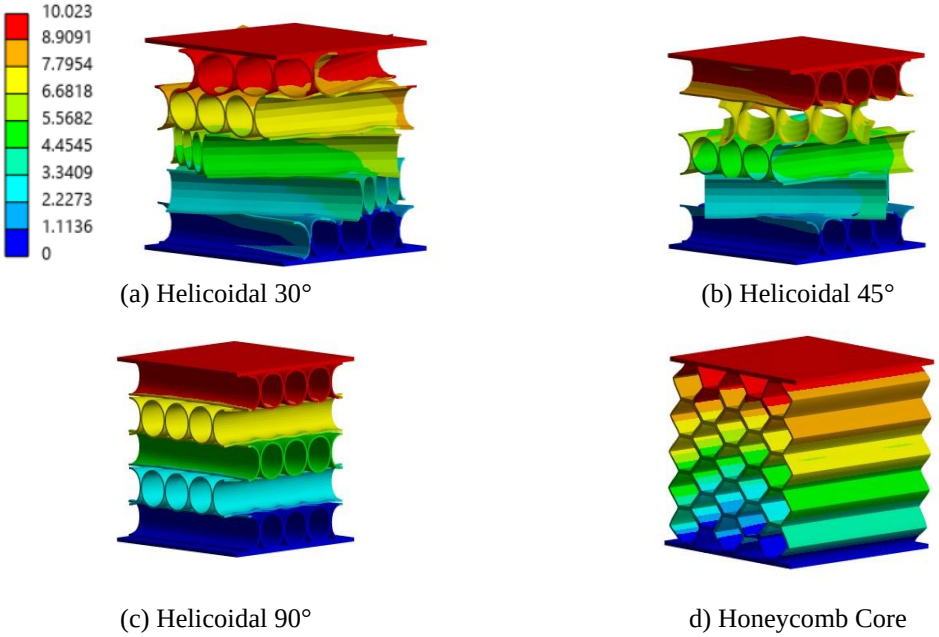

(a) Helicoidal 30° (b) Helicoidal 45°

(c) Helicoidal 90° d) Honeycomb Core

Figure 2. Total deformation contours for the four core architectures under quasi-static compression.

of thin-walled hexagonal cells that undergoes controlled buckling under load application. 90° helicoidal configuration exhibited the lowest deformation, indicating its high stiffness among the configurations. As the ply orientation reaches 90°, load transfer becomes more different and less dependent on the internal structural configurations, resulting in reduced displacement which was also observed in bouligand-type and high-angle helicoids.

Overall, the deformation result indicates the clear structural performance gap cause by the ply rotation angle, where the helicoidal architectures with lower angle rotation exhibit better compliance, whereas 90° structure provides comparatively stiffer response. Therse findings offer a substantial basis for selecting core designs according to desired deformation capacity.

5.1.2 Equivalent stress

Fig. 3(a-d) Shows Stress distribution of the four core architectures under quasi-static compressive displacement of 10 mm shows a clear structural difference among them in load transfer and stress localisation. The maximum stress values obtained were 56350 MPa for the helicoidal 90° structure, 53290 MPa for the honeycomb core, 52880 MPa for the helicoidal 45° structure, and 50003 MPa for the helicoidal 30° structure. The helicoidal 90° structure exhibited the highest stress, reflecting its relative stiff configuration and reduced capacity for redistribution of shear. When the ply rotation angle is large adjacent layers are near linearly arranger with orthogonal orientations, thus constraining the interlayer sliding and promoting simple way of axial load transfer. This results in great stress magnitudes and sharper concentration points. The honeycomb structure follows a similar pattern of axial load transfer to its adjacent cells which recorded a moderately high stress value, as for honeycomb structures this is consistent with thin-walled hexagonal cells that localises the deformation through bending of walls and junctions. Although this structure has a high stiffness-to-weight ratio, they often exhibited high stress near the

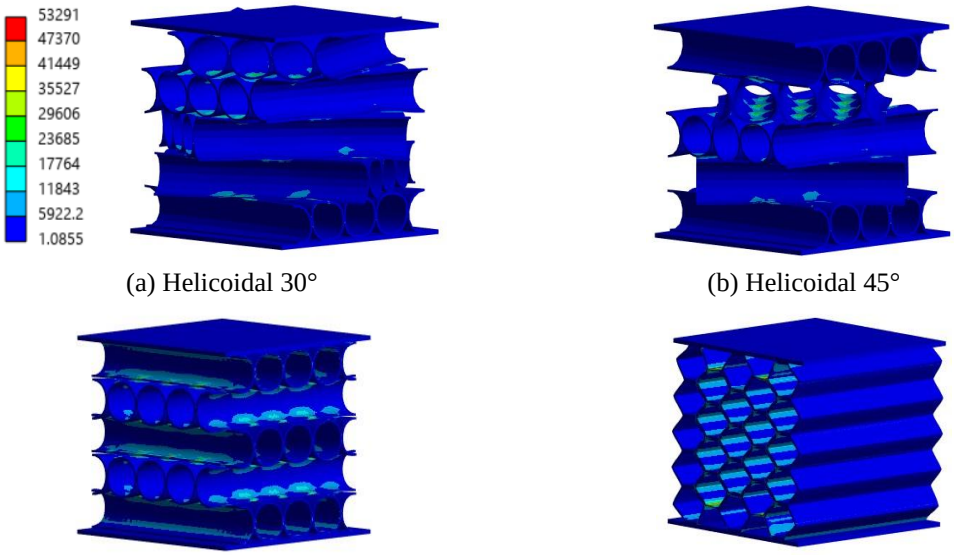

(a) Helicoidal 30° (b) Helicoidal 45°

(c) Helicoidal 90° d) Honeycomb Core

Figure 3. Equivalent von Mises stress distribution for the four core architectures

edge of the cells during compressive loading. By comparison, the helicoidal 30° and 45° structures displayed lower stress contours. Smaller rotation increments promote more gradual fibre orientation across layers allowing stress to disperse through a twisting path. This mechanism reduces the localized stress and enhances the structure's ability to distribute forces, a behaviour observed in biological composites such as mantis shrimp and fish scales [2, 5]

Overall, the equivalent stress results demonstrate that the helicoidal structures effectively modulates stress concentration through their rotational design once again highlighting the impact of layer rotations.

5.1.3 Equivalent strain

Fig. 4(a-d) Illustrates Equivalent Strain fields obtained from the quasi-static compression provides further insight to deformation behaviour and energy dissipation mechanisms of these structures. The maximum strain value was 2.405 for helicoidal 30° structure, 2.320 for the helicoidal 45°, 2.210 for the Honey- comb, and 2.192 for helicoidal 90°. These results show a systemic reduction in strain magnitude as the ply rotation increases, consistent with helicoidal architecture in controlled deformation. Among these structural configurations, the helicoidal 30° exhibits the highest strain, indicating its ability to undergo twisting and layer-interaction deformation. Smaller rotation increments promote a more continuous redistribution of strain to adjacent layer, and let the structure to deform uniformly while storing significant amount of strain energy. Similar behaviours are widely reported in natural Bouligand-type systems, where even a small rotation enhances the deformation capacity of a system.

Helicoidal 45° structure has shown considerable amount high strain, reflecting the balance between the shear pathways and structural rigidity as the angle grows. The deformation patter remains un- even across multiple layers, but localised strain is even and continuous compared to other structures. Honeycomb core has been a distinct strain profile characterised by their moderate

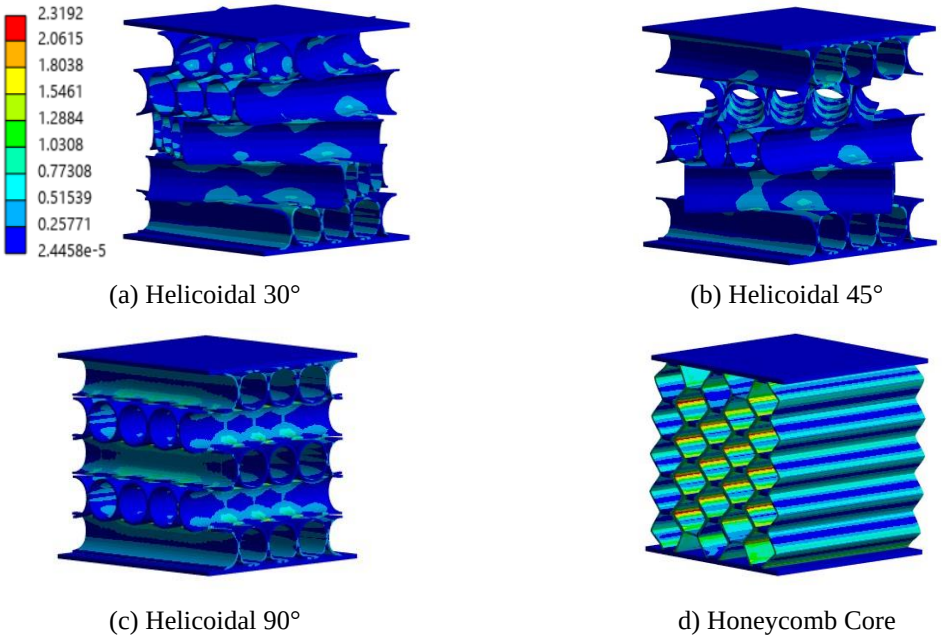

(a) Helicoidal 30° (b) Helicoidal 45°

(c) Helicoidal 90° d) Honeycomb Core

Figure 4. Equivalent strain of the structural configurations

strain levels con- centrated along the cell walls and junctions. This behaviour aligns with the mechanics of thin-walled structures, where compressive deformation initiates wall bending followed by localised stretching. Helicoidal 90° structure exhibits the lowest equivalent strain, as they are more consistent on their relatively stiff orientation and reduce interlayer mobility. Larger rotation angles directly alter the directionality of adjacent layers, thus suppressing deformation and limiting the strain accumulation [7, 8]

Overall, the strain results show the role of ply orientation as a key design parameter that governs the deformation, with smaller rotation being to accommodate greater strain under quasi-static compression.

5.1.4 Strain energy

Fig. 5(a-d) Shows Strain energy accumulation within the structural configurations during quasi-static compression analysis indicates the measure of its ability to absorb work before any damage or catastrophic failures.

The maximum strain energy recorded was 19.809 mJ for the helicoidal 30° structure, 18.221 mJ for the helicoidal 45°, 17.096 mJ for the honeycomb structure, and 16.391 mJ for helicoidal 90°. The helicoidal 30° architecture shows the greatest sing of strain energy, reflecting its enhanced compliance and capacity for disturbed deformation across layers. Lower rotational increments generate smoother transitions between adjacent plies; these arrangements enhance toughness and energy dissipation through progressive failure mechanisms.

The helicoidal 45° structure demonstrates high strain energy as it is slightly stiffer than the 30° configuration, it still maintains sufficient interlayer rotations to facilitate energy dissipation through bending and shear deformation.

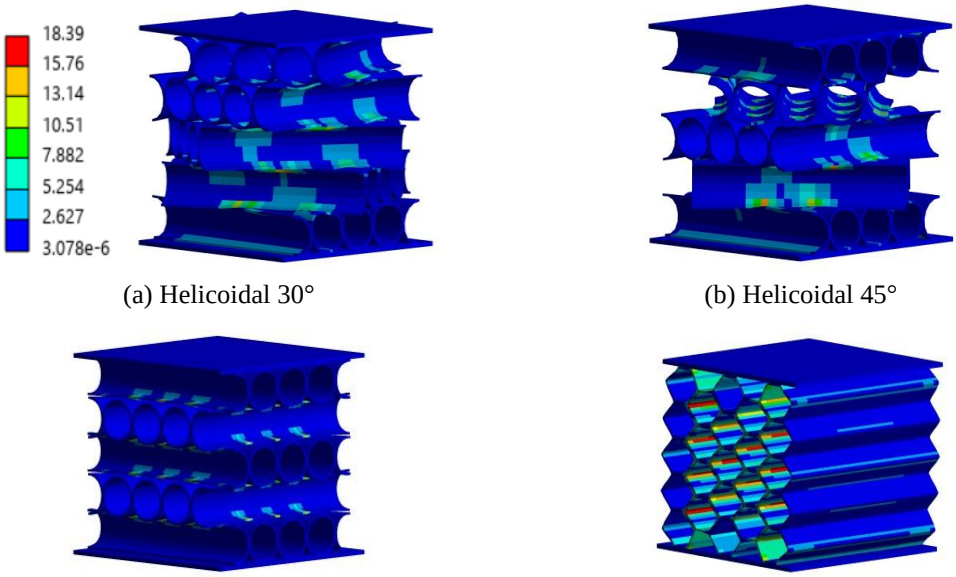

(a) Helicoidal 30° (b) Helicoidal 45°

(c) Helicoidal 90° d) Honeycomb Core

Figure 5. Strain energy distribution across the architectures

The honeycomb core exhibits lower strain energy compared to the helicoidal configurations, as it is consistent with predominantly bending-dominated deformation mechanism. Although they offer favourable stiffness-to-weight ra- tios, their ability to store strain energy is limited by localised cell-wall bending and node stress concentration. Helicoidal 90° structure records the lowest strain energy due to its rigid orientation. Larger rotation angles constrain interlayer energy storing. Similar trends have been reported in high- angle helicoidal laminates that prioritise stiffness over energy dissipation [4, 10]

Overall, the strain energy result highlights the superior energy-absorbing capability of small-angle helicoidal laminates, indicating the importance of rotational design in impact-resistant systems.

5.2 Flexural (bending) response

In addition to compressive loading, the flexural behaviour of the helicoidal and honeycomb structures was investigated to evaluate their structural performance under bending action. This analysis was conducted to represent more realistic service conditions where structural components are subjected to combined axial and flexural loads.

A displacement-controlled bending load of 2 mm was applied at the top plate, while the bottom plate was constrained to simulate a flexural loading condition. Similar material properties, meshing parameters and contacts are used to ensure consistency and to enable direct comparison between these loading cases.

The 45° helicoidal structure shows a balanced response with moderate deformation and a relatively uniform stress distribution across the all the layers of the arrangement. Whereas the30° configuration exhibited a slightly higher compliance, with increased deformation while maintaining stress levels.

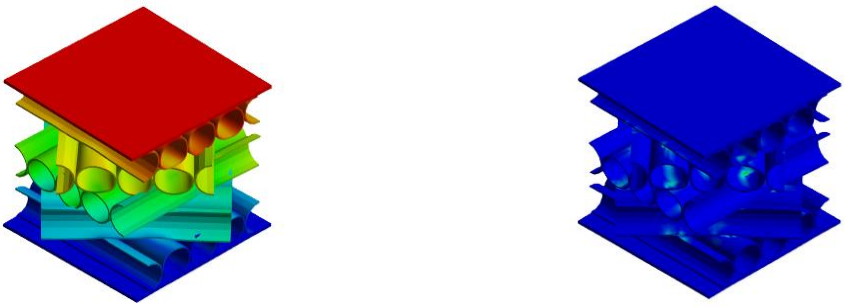

(a) Total deformation (b) Equivalents von-Mises stress

Figure 6. Representative flexural response of the 45° helicoidal structure under controlled displacement

The 90° helicoidal configuration also showed higher stress concentration under bending, mainly due to its directional stiffness that limited the stress redistribution across layers. In contrast, the honeycomb structure exhibited increased internal deformation with bending mechanisms, resulting in comparatively in a higher strain energy absorption compared to other structures.

Overall, these results suggest that the helicoidal configurations provide improved stress distribution and structural balance under bending conditions and honeycomb exhibits a distributed deformation which contributes to its moderate energy absorption. These findings align with the compressive analysis and shows the influence of structural architecture on flexural performance. Among the investigated configurations, the 45° helicoidal structure is illustrated as a representative case in Fig. 6(a-b) due to its balanced flexural response, demonstrating controlled deformation and efficient stress redistribution.

6. Comparison of the structural configurations

6.1 Comparison under compressive Loading

A comparative evaluation of the four structural architectures was performed using the interpolated response derived curve from the simulation results, Fig. 6. Illustrates the evolution of deformation, equivalent stress, equivalent strain, and strain energy across all 20 steps with all exhibiting the linear progression due to the applied quasi-static displacement except strain energy as it follows the expected quadratic trend.

The deformation plot shows a clear separation between these configurations, with helicoidal 30° structure consistently producing the highest deformation at each load step, followed by 45° and honeycomb structures. The 90° remains the stiffest throughout the loading path, thereby producing the least deformation across all those configurations as shown in Fig. 7(a). The hierarchical order:

30° > 45° > Honeycomb > 90°

Stress curves show the highest value for the 90° configuration, reflecting tis stiffness and reduced deformation capability. The honeycomb and 45° exhibit moderate amount of stress levels, with 45° and 30° configuration maintains the lower-level stress concentrations. This behaviour corresponds well with published findings of helicoidal and cellular architectures as shown in Fig. 7(b).

The hierarchical order:

90° > Honeycomb ≈45° > 30°

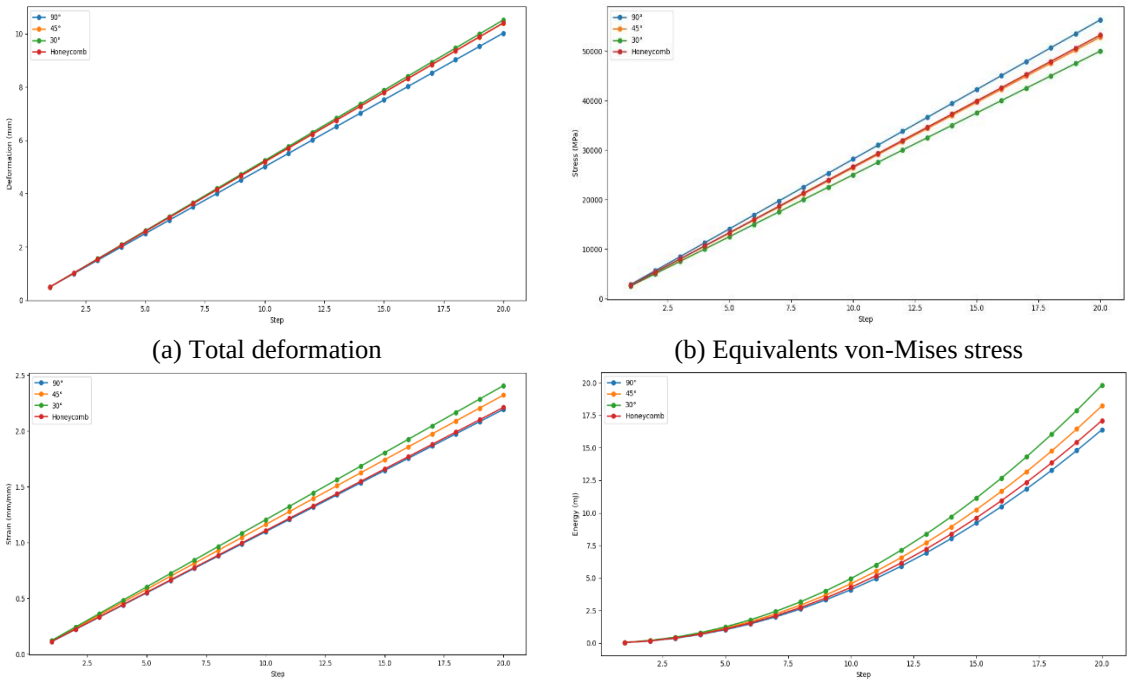

(a) Total deformation (b) Equivalents von-Mises stress

(c) Equivalent strain (d) Strain energy

Figure 7. Comparative performance metrics of the four core architectures

Strain trends mirror deformation curves, reinforcing that strain accumulation is strongly governed by the rotational increment in helicoidal stacking. Again, 30° structure demonstrates superior strain capacity, consistent with mechanisms reported in biological composites such as crustacean exoskeletons as shown in Fig. 7(c). The hierarchical order:

30° > 45° > Honeycomb > 90°

Strain energy curve further confirms this hierarchy. The quadratic scaling highlights the enhanced energy absorption of 30° and 45° helicoids, relative to both honeycomb and 90° structures. This is consistent with literature showing that smaller-angle helicoids provide enhanced energy dissipation as shown in Fig. 7(d). The hierarchical order:

30° > 45° > Honeycomb > 90°

6.2 Comparison under flexural loading

A comparative evaluation of the four structural architectures was performed under displacement-controlled bending. The maximum total deformation, equivalent stress, equivalent elastic strain, and strain energy were extracted from the simulation results. Fig. 8 presents the normalized flexural performance comparison (45° configuration taken as reference), while Table 4 summarizes the corresponding maximum response values.

The deformation results reveal a clear distinction among the configurations. The 90° structure exhibits the lowest displacement under bending, reflecting its higher flexural stiffness. The 45° configuration demonstrates moderate deformation, while the honeycomb structure shows slightly higher compliance. The 30° helicoidal configuration produces the highest deformation under the

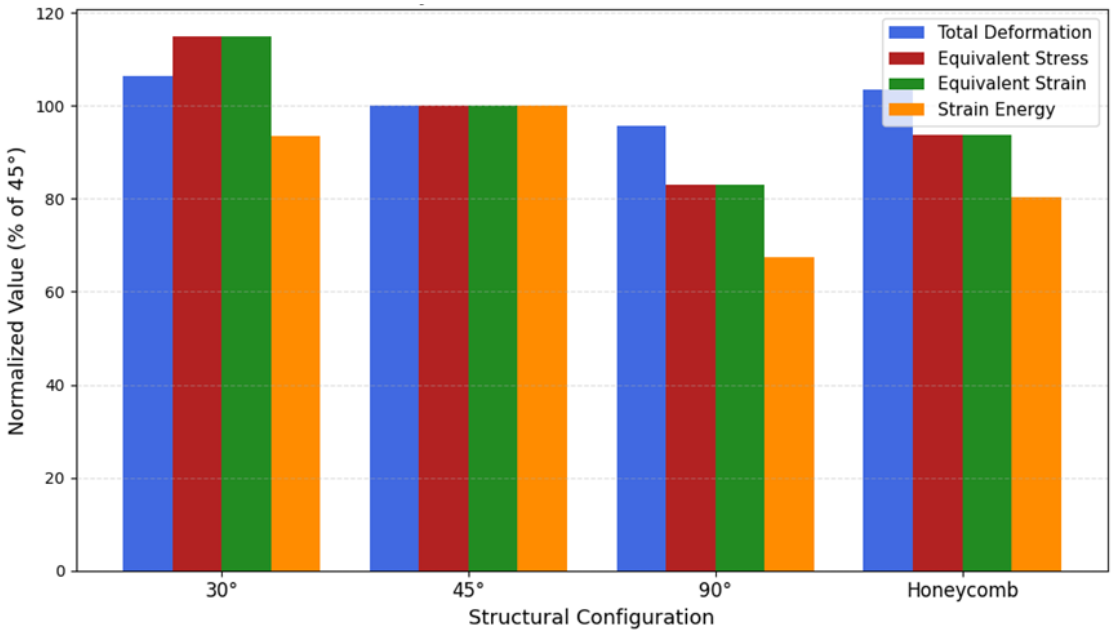

Figure 8. Normalized flexural performance comparison of the investigated architectures (45° configuration = 100%)

Table 4. Maximum flexural response values for the investigated structural configurations under displacement-controlled bending

Structure	Total Deformation (mm)	Equivalent Stress (MPa)	Equivalent Strain (–)	Strain Energy (J)
30° Helicoidal	2.18	2133	0.0054	0.43
45° Helicoidal	2.05	1856	0.0047	0.46
90° Helicoidal	1.96	1540	0.0039	0.31
Honeycomb	2.12	1738	0.0044	0.37

same loading condition. The hierarchical order is:

90° < 45° < Honeycomb < 30°

The stress distribution follows a similar structural trend. The 90° configuration showed the lowest equivalent stress due to its directional stiffness. The honeycomb structure also showed moderate stress levels, followed by the 45° configuration, while the 30° helicoidal structure shows the highest stress response under bending. The hierarchical order is:

90° < Honeycomb < 45° < 30°

Equivalent Strain results follow the same trend as deformation. The 90° configuration demonstrates the lowest elastic strain indicating its reduced internal deformation. The honeycomb and 45° structures maintain intermediate strain levels, whereas the 30° configuration shows the highest strain under bending. The hierarchical order is:

90° < Honeycomb < 45° < 30°

The energy result shows the differences in elastic energy storage capability. The 45° helicoidal configuration exhibits the highest strain energy absorption, indicating its improved load redistribution. The 30° structure follows, while the honeycomb configuration shows moderate

energy storage. The 90° structure presents the lowest strain energy due to its higher stiffness and reduced deformation. The Hierarchical order is:

45° > 30° > Honeycomb > 90°

Overall, while the 90° configuration provides the maximum stiffness under bending, but it does not optimize energy absorption. The 30° configuration accommodates higher deformation trading with increased stress and strain demand. The honeycomb architecture demonstrates moderate structural behavior. By considering balanced deformation control, stress distribution, and elastic energy absorption, the 45° helicoidal configuration exhibits the most efficient structural performance under flexural loading without inducing damage.

7. Conclusions

This study investigated the quasi-static compression and flexural response of three helicoidal architectures 30°, 45°, 90°, and a Honeycomb structure using finite element modelling. Despite their geometric differences in layer arrangement and rotational sequence, all these four structures demonstrated consistent structural behavior trends aligned with the observed results of natural Bouligand-type systems.

• The controlled varying of ply rotation enabled clear indication of how helicoidal angle arrangement governs the stiffness, deformation and energy absorption capability. Results obtained also confirms that ply rotation angle is the dominant parameter that controls mechanical performance in these structures. Smaller rotational angle enhances deformation and energy dissipation, while larger angles increase the stiffness at the expense of strain accommodation. These findings support biological observations of natural Bouligand-type structures to optimize toughness through gradual rotational twist rather than just orientation shifts [8]

• Overall, this study demonstrates that optimizing the helicoidal angles offers a high means of turning mechanical performance of such helicoidal structures. The numerical values presented here provide a foundation for future optimization, including gradient helicoidal stacking, variable wall thickness, and experimental validation. The comparative performance of these configurations aligns closely with the trends reported across multiple findings in the field of bio-inspired architected materials.

• The smaller-angles helicoidal structures consistently demonstrated higher deformation, larger equivalent strains, and increased strain energy, which corresponds with the deformation mechanisms observed in natural Bouligand-type systems. In such biological structures, gradual rotational increments enhance the shear distribution and delays the of localized failures, resulting in improved toughness [2, 8].

• In addition to Compressive load analysis, the comparative flexural analysis demonstrated that while the 90° configuration provides maximum stiffness under bending, the 45° helicoidal structure achieves the most balanced structural response by combining controlled deformation with enhanced elastic energy absorption. This confirms that helicoidal angle selection governs performance not only under axial compression but also under flexural loading conditions.

References

1. Nguyen, T.D., Pham, H.T., Tran, Q.H. (2023). Computational continuum modelling of advanced composite structures. Advances in Computational Design, 8(1), 77-96. https://doi.org/10.12989/acd.

2023.8.1.077
2. Raabe, D., Sachs, C., Romano, P. (2005). The crustacean exoskeleton as an example of a structurally and mechanically graded biological nanocomposite material. Acta Materialia, 53(15), 4281-4292. https://doi.org/10.1016/j.actamat.2005.05.027
3. Lee, K.S., Choi, Y.J., Wang, L. (2022). Finite element modelling of layered and sandwich composite structures. Advances in Computational Design, 7(3), 253-279. https://doi.org/10.12989/acd.2022.7.3.253
4. Weaver, J.C., Milliron, G.W., Miserez, A., Evans-Lutterodt, K., Herrera, S., Gallana, I., Mershon, W.J., Swanson, B., Zavattieri, P., Kisailus, D. (2012). The stomatopod dactyl club: A formidable damage-tolerant biological hammer. Science, 336(6086), 1275-1280. https://doi.org/10.1126/science.1218764
5. Suksangpanya, N., Yaraghi, N.A., Kisailus, D., Zavattieri, P.D. (2017). Twisting cracks in Bouligand structures. Journal of the Mechanical Behavior of Biomedical Materials, 76, 38-57. https://doi.org/10.1016/j.jmbbm.2017.06.003
6. Kim, J.H., Park, S.H., Lee, D.H. (2023). Numerical investigation of architected composite structures under quasi-static compression. Advances in Computational Design, 8(2), 113-131. https://doi.org/10.12989/acd.2023.8.2.113
7. Han, Q., Wu, H., Zhang, J., Li, D. (2020). Study on impact resistance behaviors of a novel composite laminate with basalt fiber for helical-sinusoidal bionic structure. Composites Part B: Engineering, 191, 107976. https://doi.org/10.1016/j.compositesb.2020.107976
8. Ning, H., Wang, Z., Liu, Y. (2024). A review of helicoidal composites: From natural to bio-inspired damage tolerant materials. International Materials Reviews, 69(3-4), 181-228. https://doi.org/10.1080/09506608.2023.2244179
9. Al-Maliki, A.F., Ahmed, R.A., Moustafa, N.M., Faleh, N.M. (2020). Finite element based modeling and thermal dynamic analysis of functionally graded graphene reinforced beams. Advances in Computational Design, 5(2), 177-193. https://doi.org/10.12989/acd.2020.5.2.177.
10. Wang, Z., Liu, Y., Zhang, X. (2024). Numerical assessment of architected cellular materials under displacement-controlled loading. Advances in Computational Design, 9(1), 53-71. https://doi.org/10.12989/acd.2024.9.1.053
11. Narwariya, M., Choudhury, A., Sharma, A.K. (2018). Harmonic analysis of moderately thick symmetric cross-ply laminated composite plate using FEM. Advances in Computational Design, 3(2), 113-130. https://doi.org/10.12989/acd.2018.3.2.113
12. Adda Bedia, E.A., Tounsi, A., Mechab, I. (2018). Finite element analysis of composite plates based on higher-order shear deformation theories. Journal of Sandwich Structures & Materials, 20(5), 613-635. https://doi.org/10.1177/1099636216676942
13. Bourada, F., Tounsi, A., Bousahla, A.A. (2018). Mechanical response of laminated composite plates using refined theories. Steel and Composite Structures, 28(3), 295-310. https://doi.org/10.12989/scs.2018.28.3.295
14. Bousahla, A.A., Tounsi, A., Bourada, F. (2019). Stress and strain analysis of functionally graded structures. Computers and Concrete, 23(4), 245-258. https://doi.org/10.12989/cac.2019.23.4.245
15. Tounsi, A., Bourada, F., Bousahla, A.A. (2019). Computational analysis of advanced composite structures under mechanical loading. Composite Structures. (In press/Online first)